Laboratory seismic measurements for layer-specific description of fluid mud and for linking seismic velocities to rheological properties

Ma, X.; Kirichek, Alex ; Shakeel, A.; Heller, H.K.J.; Draganov, D.S.

DOI
10.1121/10.0005039

Publication date
2021

Document Version
Final published version

Published in
The Journal of the Acoustical Society of America

Laboratory seismic measurements for layer-specific description of fluid mud and for linking seismic velocities to rheological properties

Xu Ma, Alex Kirichek, Ahmad Shakeel, Karel Heller, and Deyan Draganov

Citation: The Journal of the Acoustical Society of America **149**, 3862 (2021); doi: 10.1121/10.0005039
View online: https://doi.org/10.1121/10.0005039
View Table of Contents: https://asa.scitation.org/toc/jas/149/6
Published by the Acoustical Society of America

JASA ARTICLE

Laboratory seismic measurements for layer-specific description of fluid mud and for linking seismic velocities to rheological properties

Xu Ma,[1,a)] Alex Kirichek,[2] Ahmad Shakeel,[2] Karel Heller,[1] and Deyan Draganov[1]

[1]*Department of Geosciences and Engineering, Faculty of Civil Engineering and Geosciences, Delft University of Technology, Delft, 2628 CN, The Netherlands*

[2]*Department of Hydraulic Engineering, Faculty of Civil Engineering and Geosciences, Delft University of Technology, Delft, 2628 CN, The Netherlands*

ABSTRACT:

The velocities of the seismic waves propagating in the fluid-mud layer are governed by the rheological properties and density of the fluid mud. Performing seismic transmission measurements inside the fluid mud can give good estimates of the seismic velocities and, thus, of the rheological properties and density. Laboratory ultrasonic transmission measurements of the wave velocities in the fluid-mud layer and their temporal evolution are shown. It is found that the shear-wave velocity and yield stress are positively correlated. Performing a seismic reflection survey for characterization of the fluid-mud layers could be more practical because it allows towing the sources and receivers above the top of fluid-mud layer. Interpretation of the results from a reflection survey, though, is influenced by the water layer above the fluid mud. Applying seismic interferometry to reflection measurements can eliminate the influence of the water layer and retrieve a reflection response from inside the fluid-mud layer. This eliminates the influence of the temperature and salinity of the water layer to obtain information about the seismic properties of the fluid-mud layer. To introduce the approach of retrieving and extracting the reflection response from inside the fluid-mud layer, data from laboratory measurements are used. The obtained compressional- and shear-wave velocities are validated by comparing them with values from current transmission measurements.

 https://doi.org/10.1121/10.0005039

(Received 9 December 2020; revised 4 May 2021; accepted 6 May 2021; published online 3 June 2021)

[Editor: Nicholas P. Chotiros] Pages: 3862–3877

I. INTRODUCTION

Surveying the fluid-mud layers in ports and waterways is of prime importance for safeguarding the navigation of maritime transport. The areas with fluid-mud layers are regularly surveyed to provide up-to-date navigation charts of the nautical bottom for incoming and outgoing vessels. Identifying the nautical bottom, though, is ambiguous and challenging (Kirby *et al.*, 2016; Kirichek *et al.*, 2018). The traditional echo-sounding techniques can typically detect the water/fluid-mud level but fail to reliably map a sharp interface between the fluid mud and the consolidated bed. Echo sounders can falsely identify the bottoms if the site shows a well-formed lutocline, i.e., an abrupt change of sediment concentration with depth (McAnally *et al.*, 2007), due to the increase in the sediment concentration at the top of the fluid-mud layer (Carneiro *et al.*, 2020).

The fluid mud can be described as a highly concentrated non-Newtonian suspension of sediment consisting mainly of water, organic matter, silt, and clay minerals (McAnally *et al.*, 2007). The fluid mud is in a transient state and in time will eventually settle and consolidate unless mixing energy is added. In ports and waterways, the mixing occurs as a result of maintenance dredging, navigation, or natural currents. The fluid mud has a weak strength, which increases over time to form a consolidated bed of considerably higher rigidity (Abril *et al.*, 2000). A fluid-mud layer can be of substantial thickness with small density gradients within the layer. Nichols (1984) suggested that the two- and three-layer models can be used as depositional bed models. The two-layer model can be applied to the fluid-mud layer with an abrupt increase in density. The three-layer model is used to describe the fluid-mud layer with a moderate increase in density. Vertical concentration and density profiles illustrate that there is a discontinuity at the water–bed interface (Nichols, 1984). These density gradients and discontinuity make it challenging to detect sufficient acoustic impedances within naturally deposited mud layers by means of traditional sounding. Therefore, other strategies have been developed for surveying the fluid-mud layers in ports and waterways. The nautical-bottom approach has been used in ports worldwide (McAnally *et al.*, 2007; Kirichek *et al.*, 2018). In this approach, the density and yield stress of the mud have been used as the physical parameters which define the nautical bottom. For instance, in navigation charts in the Port of Rotterdam and the Port of Emden, instead of the

[a)]Electronic mail: x.ma-5@tudelft.nl

water/fluid-mud level, the levels of 1.2 kg/l and 100 Pa are used, respectively. These levels are chosen based on the combination of seismic data and yield stress/density vertical profiles, which are measured in a water-mud column by mud profilers (Kirichek *et al.*, 2020).

One of the goals of our study is to investigate whether the density and yield stress can be estimated from seismic data alone. For that, a relationship between the seismic response and geotechnical behavior of marine sediments should be found. Having such a relationship will further show how seismic measurement could be used as a reliable tool to map the interface between the fluid mud and solid mud under it, helping to identify the nautical bottom and ensure safety while at the same time maximizing navigability. We develop seismic transmission measurement and reflection measurement to estimate the seismic velocities of fluid mud. We also investigate the seismic-velocity variations with yield stress obtained from rheological measurements to look for possible relations.

As a step forward in that direction, it is necessary to rigorously measure the seismic velocities of fluid mud using laboratory tests because the empirical relationships of the wave properties established for coarse-grain sediments cannot be applied to fluid mud because of the composition of the muddy sediments (Ballard *et al.*, 2014). The density of the fluid mud changes as the fluid mud settles. It is interesting to know whether this change is sufficiently high to be clearly detected by seismic measurements and, if yes, which waves—compressional (P) or shear (S)—are better suited for sensing this change.

The easiest way to investigate the relation between the wave properties and density and yield stress is to perform direct transmission measurements. In a laboratory, performing direct transmission measurements with a point-to-point measurements setup is easy and reliable because homogeneous mud samples can easily be produced and because of the limited scale of the measurements. The P- and S-wave velocities depend on the effective stress. Leurer (2004) conducted pulse-transmission measurements with a center frequency of 50 kHz and reported that the P-wave (compressional wave) velocities range from 1840 to 2462 m/s in a foraminiferal mud at 20 MPa. Using a center frequency of 100 kHz under different effective pressures, it was also found that the S-wave (shear wave) velocities range from 450 to 975 m/s (Leurer 2004). In addition to the effective stress, the S-wave velocity is affected by other factors, including the measurement technique, sediment type, textural differences of the sediment, grain size, and cementation (Bowles 1997). Other studies presented seismic transmission tests for measuring P- and S-waves with low center frequencies on mud samples that are prepared by mixing dry kaolinite with distilled water (Ballard *et al.*, 2014; Ballard and Lee, 2016). It was reported that the P-wave velocity for a center frequency of 90 kHz is about 1460 m/s, whereas the S-wave velocity for a center frequency of 200 Hz is just 7 m/s. Thus, seismic transmission measurements in laboratory settings are necessary for characterizing mud samples because the seismic velocities of muddy sediments change significantly, depending on the mud samples and center frequencies used for the measurements. Using physics-based models is challenging for predicting seafloor seismic properties (Jackson and Richardson, 2007). Empirical models (Hamilton, 1979) and physics-based models (Stoll, 1977; Buckingham, 1997; Buckingham, 2005; Chotiros, 2021) can be used to predict the propagation velocities of waves.

In practice, exploration in the field using transmission measurements would require traveltime tomography between different "borehole-like" observations at multiple points to obtain reliable three-dimensional (3D) information of the velocities. If the points for transmission measurements extend also to the water layer, the tomographic inversion can be used to map the water/fluid–mud interface. Although exploration with transmission measurements are feasible, a more practical way for investigating sediments in ports and waterways would be to use a boat that tows sources and receivers in the water for a reflection survey, as commonly used by the resource-exploration industry. A reflection survey will also allow the mapping of the depth of the water/fluid–mud interface. There are certain requirements in ports and waterways that would need to be complied with when using seismic reflection measurements. One practical requirement is to keep the sources and receivers at a certain distance above the top of the fluid-mud layers for two reasons. First, the surface of the sediments in ports and waterways is not completely flat and, thus, towing at a certain height above the sediment surface can avoid disturbing the fluid mud. Second, a lot of unpredictable obstacles that move with the water flow at the top of the fluid mud can damage the seismic equipment during a survey. Although the reflection survey will allow the mapping of the water/fluid–mud interface, it will make the characterization of the fluid-mud layer more involved. This is so because a reflection arrival that has traversed the fluid mud will also contain parts that have propagated through the water. The part inside the water is substantially affected by the temperature and salinity of the water. By removing the water-propagation part, the influence of the changing water conditions in the processing and analysis of the reflection recordings can be eliminated.

A promising method for removing the water portion of a reflected signal is seismic interferometry (SI). Most often, this method is used to retrieve new seismic recordings between receivers from the cross correlation of existing recordings at those receivers (e.g., Shapiro and Campillo, 2004; Wapenaar and Fokkema, 2006; Draganov *et al.*, 2009). The retrieved recordings contain physical arrivals. When the assumptions underlying the application of the SI relations are not met, though, the retrieved results will also contain nonphysical arrivals (Wapenaar and Fokkema, 2006). An important condition for SI by cross correlation is that the receivers are homogeneously illuminated by the surrounding sources. When the illumination is from a preferred direction, for example, as for a reflection seismic survey with sources and receivers at the Earth's surface,

nonphysical arrivals are retrieved due to internal scattering inside the subsurface layers (Snieder *et al.*, 2006). Such nonphysical arrivals actually represent reflections inside the layers or a stack of several layers. Draganov *et al.* (2012) and King and Curtis (2012) investigated the application of SI in marine surveys to specifically use nonphysical (ghost) reflections to estimate the layer-specific propagation velocities for layers in the subsurface. Below, we aim to use SI with laboratory seismic reflection measurements to validate the potential of using ghost reflections for fluid-mud characterization and monitoring by eliminating the influence of the water layer. The reflection measurement in the laboratory can provide better control of the geometry and interface roughness compared to the field measurements. Furthermore, most of the laboratory reflection measurements only used sandy sediments; therefore, measurements with fluid mud are essential.

The second aim of our seismic experiments is to investigate whether the propagation velocities of P- and S-waves change with the settling of fluid mud and quantify the possible velocity changes during the settling process. We investigate the temporal evolution of the fluid-mud sample using the seismic transmission measurements. We perform transmission measurements to monitor the time of the first arrivals of the P- and S-waves and determine the velocities based on the travel distance and traveltime between the source and receiver.

II. DATA AND METHODS

In the following, we first introduce the preparation and handling of the fluid-mud samples (Sec. II A). We then show the measurement setups used and the methods applied for measuring the reflection (Secs. II B and II C), as shown in Fig. 1, and transmission (Sec. II D) ultrasonic data, as well as the rheological parameters and density (Sec. II E).

A. Fluid-mud preparation and handing

In this study, we use natural-mud samples collected from the Calandkanaal in the Port of Rotterdam. The density of the samples when extracted in the field is 1197 kg/m^3, on average, but increases with settling time. In Fig. 15 in the Appendix, we show the summary of the particle-size distributions of the fluid-mud samples that we use. During the process of collection, delivery, and storage, the mud samples may become compacted and, consequently, the porosity may reduce and the density may increase. Because of that, the first step in our laboratory experiments is to homogenize the mud samples before conducting the seismic transmission measurements and reflection measurements; i.e., the sample mud is mixed to make it homogeneous before performing the measurements. In parallel experiments, we characterize the rheological properties (i.e., yield stress and viscosity) and analyze the development of these properties during the settling of the mud. The different types of measurements are synchronously performed in consecutive days. Specifically, we conduct the rheological experiments on fluid-mud samples from day 0 to day 32, the seismic transmission measurements from day 0 to day 18, and the seismic reflection measurements from 0 to day 12, where day 0 is the same for the three measurements.

B. Seismic reflection measurements

We develop a seismic reflection system and perform fluid-mud reflection measurements with it. The system consists of four components: a fluid-mud tank, a signal-control part, ultrasonic transducers, and a transducer position manipulator (Fig. 2). The signal-control part consists of a waveform generator, power amplifier, and oscilloscope [Fig. 2(a)]. The waveform generator is used to produce signals with a specific form and frequency. In our case, we use a sine signal with a center frequency at 100 kHz, which has a length of one period. From the waveform generator, the

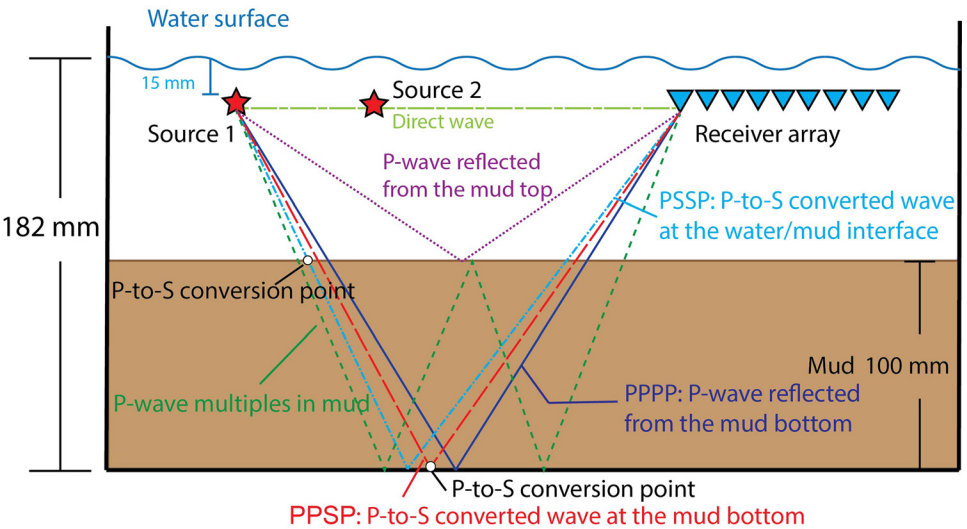

FIG. 1. (Color online) Sketch of the reflection-measurement geometry and travelpaths of the different expected wave-type arrivals. The travelpaths are only illustrative and do not represent the actual propagation travelpaths.

https://doi.org/10.1121/10.0005039

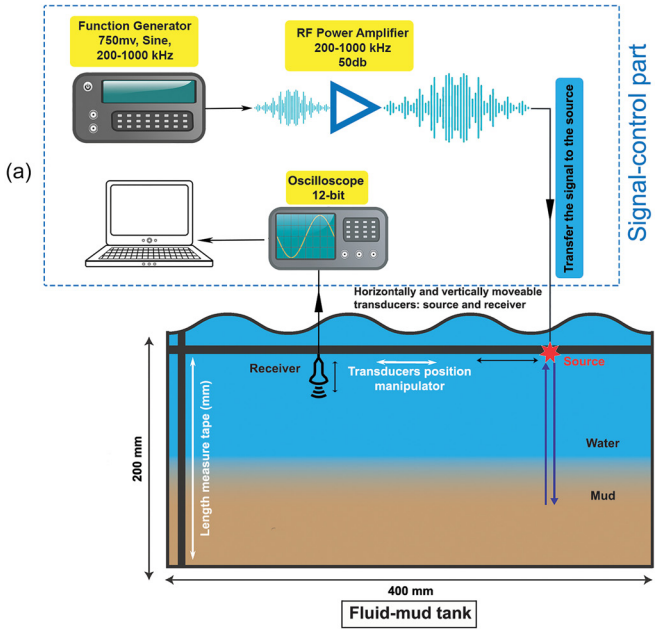

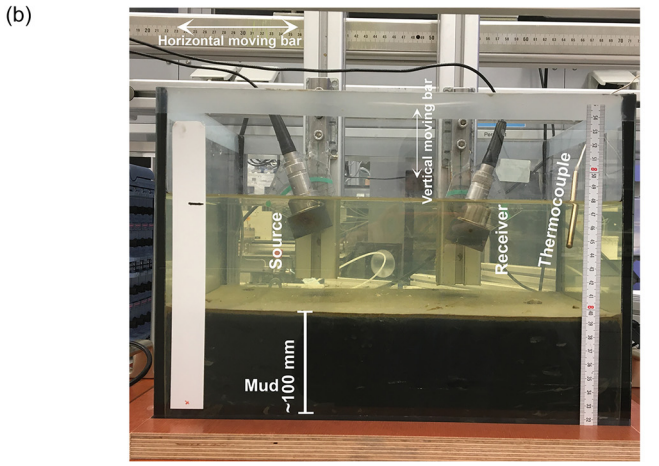

FIG. 2. (Color online) The seismic-reflection measurement system. (a) Sketch of the seismic-reflection measurement system depicting the fluid-mud tank, signal-control part, and ultrasonic-transducer position manipulator. The red star indicates the source and the black probe indicates the receiver. Arrows in blue and white indicate that the source and receiver can move vertically and horizontally, respectively. (b) The laboratory setup for the reflection measurements showing the fluid-mud tank, source and receiver ultrasonic transducers, and the position-manipulator system. Fluid mud and water are poured in the tank as one mixture and form a layered structure after the mud settles. This layered structure can be used as a proxy for mimicking the structures of underwater sediments in ports. We use a pair of piezoelectric *P*-wave transducers as a source and receiver. The transducers are placed in an adjustable rubber casing to help concentrate and emit the signal energy toward and then receive energy mainly coming from the fluid-mud layer. The source and receiver are installed on rotators attached with sliders on two vertical bars, which are connected to a main horizontal bar. The position of the transducers can be adjusted as desired for better results. Both transducers can move in the horizontal and vertical directions for changing the offset and elevation, respectively. The transducers can also rotate for changing the incidence angle from 0 deg to 90 deg and, thus, partly compensate for the transducer directionality. The sliders can be displaced along the vertical bars. The vertical bars are, in turn, attached with sliders to the main horizontal frame so that the vertical bars can be moved along the horizontal frame and, hence, change the horizontal position of the transducers.

signal is sent to the amplifier, where the signal energy is boosted to counteract the significant attenuation of the signals when propagating through the mud layers. After the amplification, the amplitudes at 63 and 129 kHz are half of the amplitude at 100 kHz. The output from the amplifier is connected to the source transducer, which sends a signal in the mud. The reflected signal is then detected by the receiver transducer from where it is fed to the oscilloscope for visualizing the waveforms. The oscilloscope is connected to a computer that uses LabVIEW software (National Instruments, United States) to plot and record the waveform data.

The fluid-mud tank is a rectangular glass tank containing the fluid mud covered with a water layer [Fig. 2(b)]. To perform the seismic reflection measurements, we follow the procedure described below.

1. Fluid-mud handling and placement

First, we deposit the homogenized mud in the tank. After placing a mud layer with a thickness of about 100 mm, we smooth the surface of the mud to ensure it is nearly flat. This is needed to avoid scattering the signals due to the roughness of the surface. After that, we gently add about 2 L of water into the tank using a pump so that the volume of water above the mud is larger than the mud volume. Before injecting the water, we cover the surface of the mud layer with an aluminum foil to bear the dynamic momentum of the water. After adding the water is finished, we slowly remove the foil. In this way, we preserve the mud surface flat.

2. Transducer adjustments

We first move the source transducer to a height slightly below the water surface. Then, we use the source transducer as a reference and adjust the position of the receiver transducer to have both of them at the same height. Measurements with the receiver are taken at several positions horizontally away from the source with the initial position closest to the source. Following each measurement, the receiver is moved horizontally away from the source with a fixed step, allowing us to create a receiver array consisting of evenly distributed receivers along the horizontal direction.

3. Data acquisition and recording

For the reflection measurements, we use two source positions, indicated by source 1 and source 2 in Fig. 1. The distance between them is 50 mm, and source 2 is closer to the receiver array. Using the steps described in Sec. II B 2 above, the receiver array is built to consist of 20 receivers with a distance between neighboring receivers of 5 mm. The offset between source 1 and the first receiver is 100 mm; the offset between source 2 and the first receiver is, thus, 50 mm. To improve the signal-to-noise ratio of the recordings at the receivers, a measurement is repeated 20 times for each source-receiver position, and the 20 measurements are

summed (stacked) to obtain a final reflection trace for this source-receiver position.

C. Seismic reflection geometry and ghost-reflection retrieval

During the seismic reflection measurements, we set the sources and receivers 15 mm below the water surface (Fig. 1). Figure 3(a) shows the recorded common-source gather (i.e., the recording at the receivers from the same source) when source 1 was used: several groups of arrivals with different temporal and amplitude distributions can be distinguished. To interpret the types of these arrivals, we compute expected arrival times of different wave types using a P-wave velocity of 1570 m/s and S-wave velocity of 958 m/s (estimated from the transmission measurements) and plot reference lines in different colors over the measured common-source gather. Seismic waves emitted from the source propagate along a variety of paths, some of which are illustrated in Fig. 1. Comparing the theoretically calculated arrival times along the illustrated paths in Fig. 1 with the recorded arrivals in Fig. 3(a), we interpret the direct P-wave (green) propagating along a straight line from the source to the different receiver positions of increasing offset. As expected from the physics of the wave propagation and directionality of the transducers, this arrival is very weak. The rest of the interpreted and color-coded arrivals exhibit hyperbolic moveout as is expected of reflected waves. We interpret the reflection from the mud top [magenta; see also Fig. 3(a)], the P-wave reflection from the mud bottom [deep blue; see also Fig. 3(a)], and the first-order internal multiple of the latter after reflection inside the mud (deep green). We also observe arrivals containing P-to-S converted portions

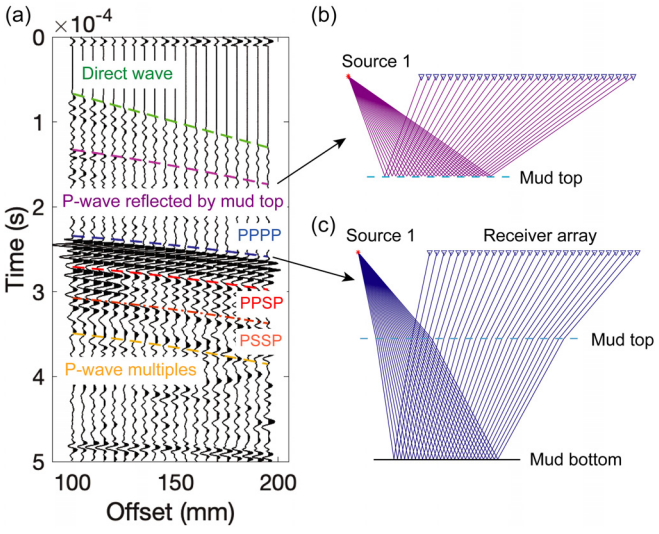

FIG. 3. (Color online) (a) The recorded common-source gather due to source 1. The different interpreted arrivals are the direct wave (green); P-wave reflected from the mud top (magenta); P-wave reflected from the mud bottom, labeled PPPP (blue); its first-order internal multiple (yellow); P-to-S conversion at the mud bottom, labeled PPSP (red); and P-to-S conversion at the water/mud interface, labeled PSSP (orange). (b) The Common-source gather recording illustrating pseudo travelpaths reflected by the mud top. (c) As in (b) but reflected by the mud bottom.

due to partial (red) and complete (light blue) propagation through the mud as S-waves. These P-to-S converted portions are generated in two ways: (1) the P-wave in the water refracts from the water layer to the mud layer and converts to a propagating S-wave; (2) the P-wave in the mud layer is reflected at the mud bottom and converts to an S-wave. Nongeometrically converted S-waves can also be generated by the water/mud interface, but for that the source should be sufficiently close to the interface (Drijkoningen *et al.*, 2012).

Among the reflections, the P-wave reflected by the mud top and three primary reflections from the mud bottom are the main targets of our study. The latter three primary reflections are generated in the following ways.

- (Deep blue) A P-wave generated by the source in the water is transmitted into the fluid-mud layer as a P-wave, reflected by the mud bottom, and continues to propagate upward until the receivers as a P-wave. We label this arrival as PPPP in our study.
- (Light blue) The P-wave from the source is converted to an S-wave at the water/mud interface, reflected by the mud bottom, and continues to propagate upward as an S-wave until the mud/water interface. We label this arrival as PSSP.
- (Red) The P-wave transmitted by the water/mud interface is converted upon reflection at the mud bottom to an S-wave, after which it continues to propagate upward as an S-wave until the mud/water interface. We label this arrival as PPSP. Note that an arrival that propagates inside the fluid mud as an S-wave only before reflection at the mud bottom, i.e., a PSPP arrival, will be recorded by the receivers at the same time as the PPSP arrival because of the homogenization of the mud.

Each of the PPPP, PPSP, and PSSP arrivals contain a water-propagation part and mud-propagation part. Removing the water-propagation part will eliminate the influences of the water salinity and temperature on the recorded arrival times. To estimate the traveltime of reflections only inside the mud in a data-driven way, we apply SI to virtually place the sources and receivers at the mud top and retrieve ghost reflections. We illustrate this process in Fig. 4.

We use two identical sources, S1 and S2, positioned at the same height and spaced 50 mm from each other. As sketched in Fig. 4, a seismic signal emitted by source S1 can follow travelpath 1–2-3–4 to be recorded by receiver R1 after being reflected by the mud bottom (solid lines in Fig. 4). In a similar way, a signal emitted by S2 can be recorded by receiver R1 after reflection from the mud top following travelpath 1–4 ft (dashed lines in Fig. 4). If the water is locally laterally homogeneous, i.e., at the scale of the length of the survey, the travelpaths 1, 1 ft, 4, and 4 ft will have the same length and will be characterized by the same traveltime. Therefore, cross-correlating the recorded trace from travelpath 1–2-3–4 with the one from 1 ft to 4 ft, i.e., applying SI, will eliminate completely the kinematics of

https://doi.org/10.1121/10.0005039

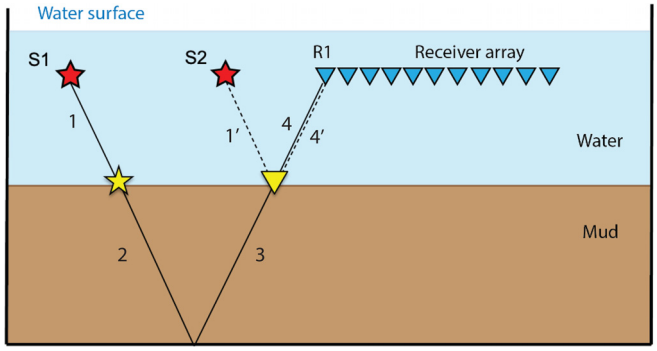

FIG. 4. (Color online) The application of SI by cross correlation in fluid-mud reflection tests. The two red stars represent the seismic sources, S1 and S2. The blue triangles represent the receiver array with the left-most receiver labeled R1. The yellow star and triangle represent the ghost source and ghost receiver, respectively, which are retrieved by cross-correlating the reflection travelpaths 1-2-3-4 from S1 to R1 and 1 ftto 4 ft from S2 to R1.

propagation through the water layer, leaving the segment 2–3 as a reflected-wave propagation only inside the fluid-mud layer. After using SI for such elimination, the segment 2–3 can be seen as a retrieved new trace that originates from a ghost source and recorded by a ghost receiver with both placed directly at the mud top (Fig. 4). In this way, S1 is virtually shifted along 1 to the mud top as the ghost source, whereas S2 is virtually shifted along 1 ft to the mud top and turned into a ghost receiver. Note that the distance between S1 and S2, their level above the mud top, and the thickness of the mud layer and propagation velocity inside it will define the exact position of a receiver for which the path through the water is eliminated. In practice, because (some of) these parameters are unknown, a summation over correlated recordings at multiple receivers should be performed, as dictated by the theory of SI, to automatically "find" the position of the sought receiver (Wapenaar and Fokkema, 2006; Draganov *et al.*, 2012). If multiple source points are used, ghost reflections at multiple offsets can be retrieved.

D. Seismic transmission measurements

We developed a seismic transmission system to measure the transmission properties of the fluid mud. The system consists of three components: a fluid-mud tank, a signal-control part, and ultrasonic transducers (Fig. 5). The signal-control part is the same as that used in the reflection measurements [Fig. 5(a)]. For the transmission measurements, though, we use a center frequency of 1 MHz. After the amplification, the amplitudes at 630 kHz and 1.29 MHz are half of the amplitude at 1 MHz.

The fluid-mud tank—a plastic box [Fig. 5(c)]—has two pairs of piezoelectric ultrasonic transducers from Panametrics (OLYMPUS, Japan) attached to two of its opposite sides [Figs. 5(a) and 5(b)]. The seismic transmission system is capable of recording P- and S-wave arrivals from P- and S-wave sources. The distance between the source transducer and receiver transducer for both pairs is 11.8 cm. We investigate the temporal evolution of the velocities and amplitudes of waves propagating in a fluid-mud sample using a center frequency of 1.0 MHz. The initial density of the fluid mud sample is 1197 kg/m^3. The seismic transmission measurements enable the direct estimation of the P- and S-wave velocities because the geometry is fixed and known and, thus, allow monitoring the time-lapsed changes with the settling of the fluid mud. Furthermore, we also use the P- and S-wave velocities estimated from the seismic transmission measurements to assist in identifying seismic wave types in the seismic reflection measurements.

E. Rheological measurements

We measure the rheological properties, i.e., yield stress and viscosity of the fluid mud, using a recently developed protocol proposed as a fast and reliable measuring tool for fluid mud (Shakeel *et al.*, 2020a,b). Yield stress is the property of fluids whereby the material does not flow unless the fluids are submitted to a stress that exceeds some critical value (Coussot, 2014). Fluidic yield stress is the minimum stress required for maintaining the flow of the undisturbed mud sample; static yield stress is the stress required for initiating the flow. The difference between these two yield points often corresponds to the Bingham yield stress. We use a HAAKE MARS I rheometer (Thermo Fisher Scientific, United States) with two measuring geometries (Couette and vane) to measure the rheological properties. In the measurement, we use two geometries and analyze the data from both of them. It is usually reported for the Couette geometry that wall slip could occur for analyzing concentrated suspensions, whereas the vane geometry is quite effective in minimizing this wall-slip effect. Moreover, the Couette geometry can significantly disturb the sample while attaining the measurement position in the cup, particularly if the aim is to estimate the consolidation effect on rheology. However, the velocity distribution is not linear within the gap between the cup and vane, particularly at higher shear rates, which sometimes limits its use. Therefore, we test both geometries to investigate a possible correlation of yield stresses obtained by both geometries with the seismic velocities. Several rheometer cups are filled with the mud samples, and each cup is used to measure the rheological behavior as a function of time. Only the fresh mud sample is stirred before the first rheological experiment; after that, the undisturbed sample is analyzed by removing the water layer from the top, as a function of time, to estimate the effect of consolidation on the yield stress. The fresh mud sample is homogenized by hand stirring before the stress ramp-up test using the rheometer. All rheological measurements were performed at 20 °C to avoid disturbance as a result of the temperature variation. We applied the stress ramp-up tests under a stress-control mode using an increasing stress from 0 to 500 Pa at a rate of 1 Pa/s until the shear rate reaches 300 s^{-1}.

In addition to the rheological properties, we also measure the density of the mud using a weight-volume method. The microstructure of the mud particles changes during the

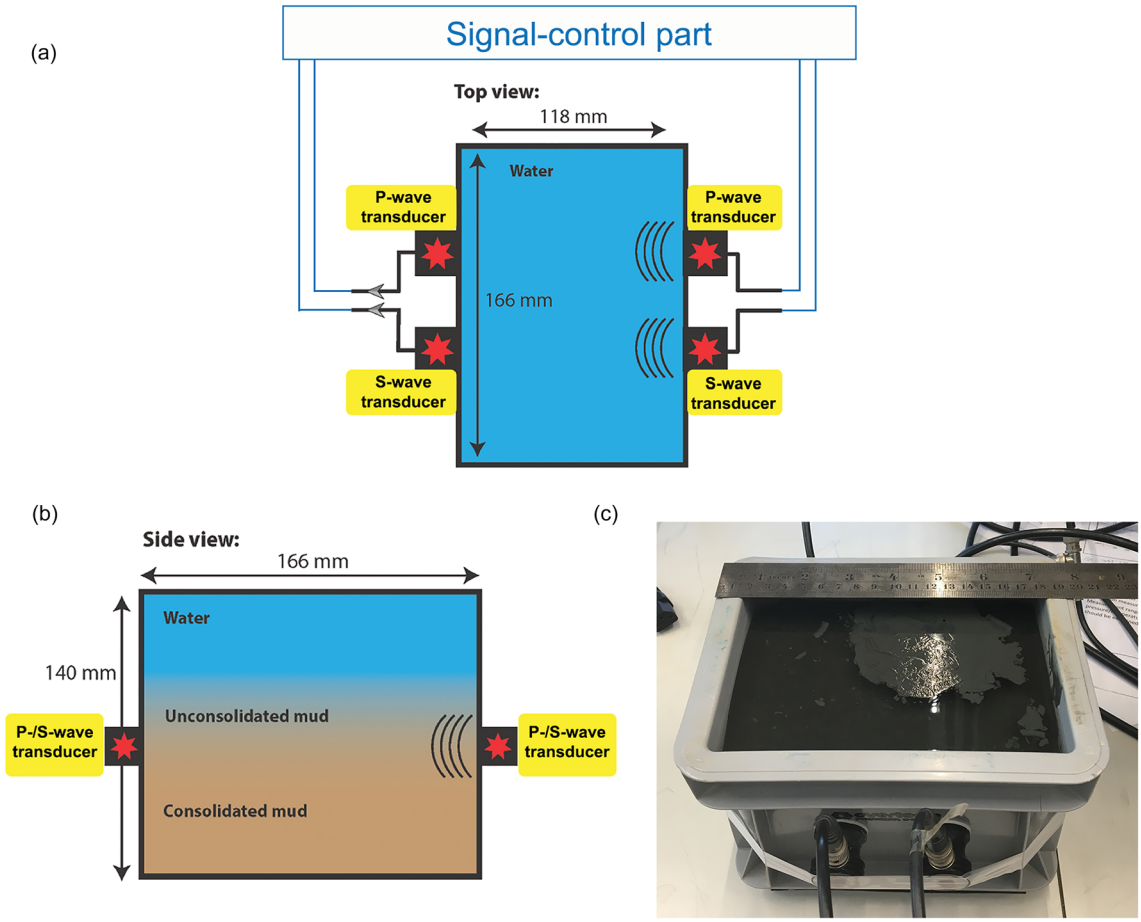

FIG. 5. (Color online) (a) Sketch of the seismic-transmission measurement system showing the top view of a box containing water and fluid mud, to which are attached ultrasonic transducers. (b) Sketch of the side view of the box with the ultrasonic transducers. (c) The photo of the actual box and transducers installed on it.

consolidation. This results in density changes, which can be attributed to the shape, orientation, spatial arrangement, and aggregations of the particle. The fluid-mud samples are dried in an oven at 105 °C for 24 h; the mass before and after oven drying is determined, giving the mass of dry solids and water content of the samples. The volumes of the water content and grains were calculated using the densities and measured masses. Last, the bulk density of a fluid-mud sample is estimated using the masses and volumes.

III. RESULTS AND DISCUSSION

We describe the results from the transmission measurements to monitor the P- and S-wave velocity variations with time in fluid mud (Sec. III A). In conjunction, we combine the velocity measurements with rheological experiments to establish a correlation between the yield stress and seismic velocities (Secs. III B and III C). We then present the results from the ultrasonic reflection measurements for monitoring with velocity semblances of velocity and energy changes in the fluid mud while it settles but also show retrieved ghost reflections (Secs. III D and III E). Finally, we compare the semblance-analysis velocity and the ghost-reflection velocity to the transmission velocity (Sec. III F).

A. Velocities and amplitudes of transmitted P- and S-waves

We find that the P-wave velocity did not show a detectable change during all measurements despite the settling effect. By using the P-wave propagation distance of 11.8 cm and time of the direct arrivals of 0.074 ms, as shown in Fig. 6, we estimate the P-wave velocity for the observation days to be 1570 m/s. We can also observe from Fig. 6 that the amplitude of the direct P-wave decreased during the temporal evolution because of the consolidation of the mud. In contrast, we find that the S-wave velocity increased with the settling time. The direct S-wave arrivals are shown in Figs. 6(a) and 6(c). Using, again, the propagation distance of 11.8 cm, we calculate the variation of the S-wave velocity with the settling process as illustrated in Fig. 8. From day 0 to day 2, there was no noticeable difference in the estimated S-wave velocity in spite of some tiny fluctuation. Starting from day 3 of settling, the S-wave velocity increased from 959 to 970 m/s and continued its increase by 25 m/s on day 4. With the strengthening of the consolidation effect, the S-wave velocity reached 1003 m/s on the last day. Thus, we find that the S-wave velocity increased by 5% during the period of 18 days of settling. The temporal change of the

https://doi.org/10.1121/10.0005039

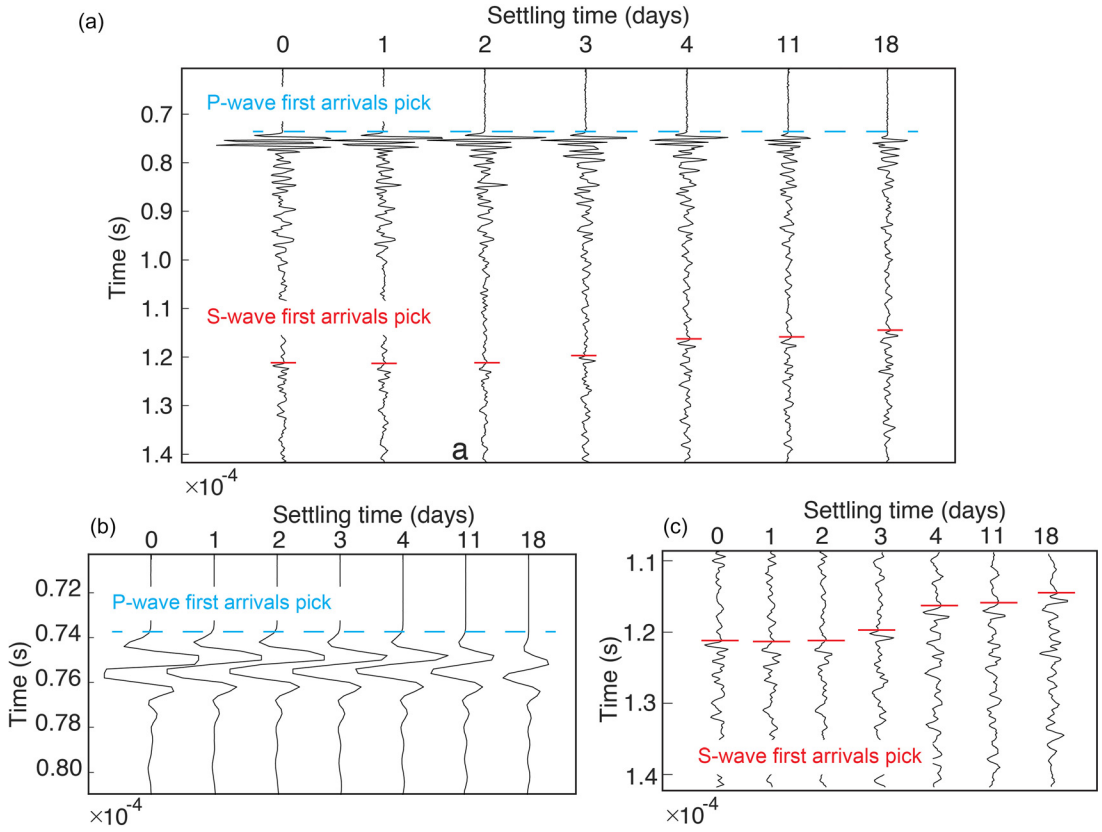

FIG. 6. (Color online) (a) The arrival time of the direct P- and S-waves using seismic transmission measurements during the settling process. Zoomed in sections of the recordings in (a) around the first arrivals of (b) the P-wave and (c) the S-wave.

S-wave velocity suggests that the settling can increase the propagation velocity of S-waves in fluid mud.

Several studies show that the S-wave velocities significantly vary (Bowles 1997). For example, many studies noted that the S-wave velocities of marine sediments are less than 700 m/s (Bowles, 1997). Kimura (2006) observed S-wave velocities of less than 100 m/s in a laboratory sample of mud without overburden pressure when using a low frequency of 2.4 kHz. Meredith (1987) found that the S-wave velocities range from 740 to 1000 m/s using the inversion results from borehole logger data from 390 to 582 m below the seafloor. In the study by Chotiros (2021), the modeling of shear-wave velocities from low to high frequencies predicts a shear-wave velocity between 100 and 200 m/s at 1 MHz for the clay sample from Eckenforde Bay and a shear-wave velocity between 400 and 700 m/s at 1 MHz for the clayey silt sample from Eel River. The measurement technique, sediment type, and cementation contribute to the fact that the S-wave velocities we observe are higher—above 959 m/s.

B. Temporal change of the density and rheology properties

We measure the density change with the settling and find that the density of the fluid mud increases with time. Bearing with the stress from consolidation, the mud particles' orientation will be perpendicular to the effective stress in the vertical direction, which further reduces the pore space and void ratio (Jackson and Richardson, 1997). The consolidation, overall, causes an increase in the density and a decrease in the porosity and permeability. This might affect the velocity of the P- and S-waves. As we can see from Fig. 7(a), the S-wave velocity appears to increase with the consolidation. Comparing the maximal and minimal values measured during the settling, we find that the density increased by 3% during the 32 days of settling [Fig. 7(b)]. We observe that the density shows a significant increase after the initial stable period of day 0–day 3. There is a strong correlation between the density and S-wave velocity after day 3. The mud samples were poured in the rheometer cups, and the rheology and density of the mud samples were analyzed as a function of time by sacrificing different cups. After day 3, the water layer on the top of the rheometer cup was first removed before the rheology and density were measured. The results show an increase in the density and yield stress. However, for days 0–3, it was not possible to remove the thin water layer from the top of the mud sample, which means there was no change in the density or water content. On the other hand, the yield stresses still increase because of the settling and consolidation process. Therefore, we think there should be an increase in the density for days 0–3 as well, which was not possible to record by using the current experimental setup.

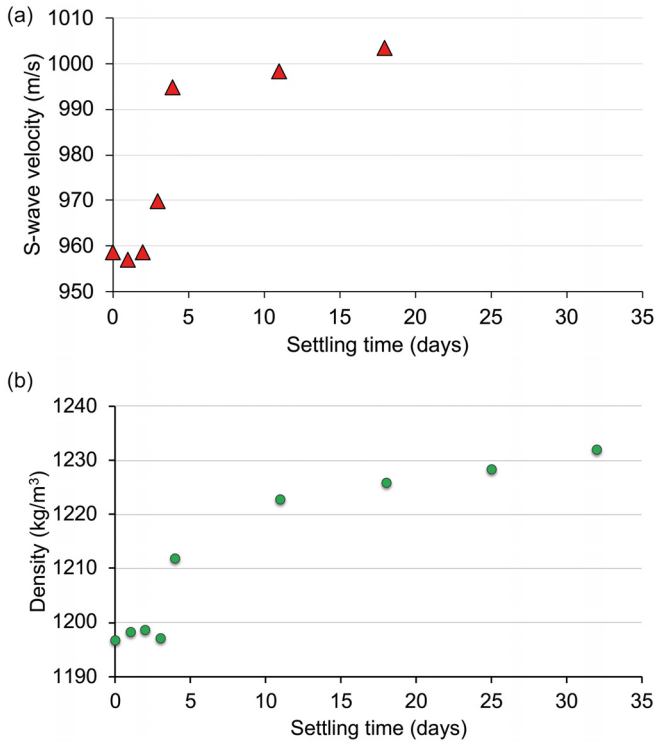

FIG. 7. (Color online) (a) The time-lapse evolution of the S-wave velocity with the settling time estimated using the seismic transmission measurements. (b) The temporal change of the density of the fluid mud with the settling time.

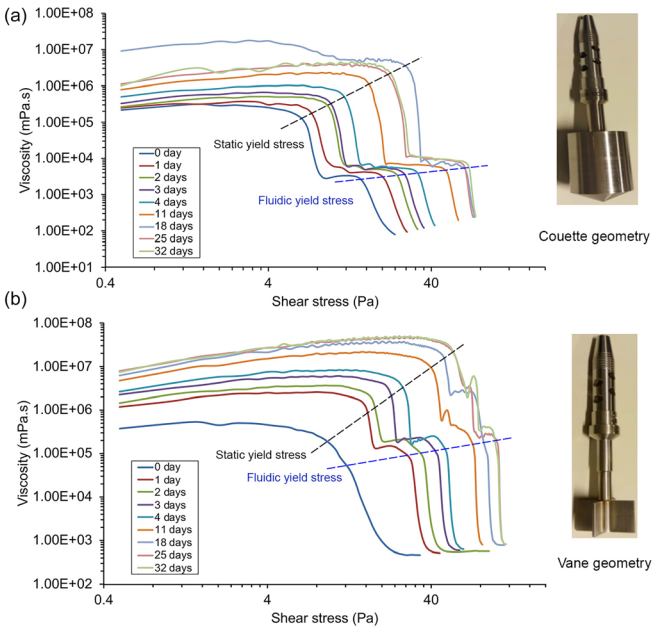

FIG. 8. (Color online) (a) The apparent viscosity versus stress obtained using measurements with the Couette geometry. (b) As in (a) but with vane geometry.

The viscosity and yield stress are monitored using stress ramp-up tests. As shown in Fig. 8, the two sharp declines in viscosity imply two kinds of yield stresses (i.e., two-step yielding). The first decline of the viscosity gives the static yield stress, whereas the second decline points to the fluidic yield stress. The graphs in Fig. 8 clearly indicate that the static yield stress, fluidic yield stress, and viscosity of the fluid-mud samples significantly increased with the settling time.

Comparing the time-lapse measurements of the fluidic yield stress using the two different measurement dimensions, we observe that using the vane geometry results in roughly 1.5 times higher values than when using the Couette geometry. This comparison verifies that the overall correlation is the same for both geometries except for a multiplication factor in yield stresses due to less disturbance of the mud sample. We perform regression analysis on the point measurements to estimate a trend of the change of the fluidic yield stress. Figure 9(a) shows that both geometries exhibit a maximum value, which is slowly approached from below following an exponential law. As shown in Fig. 9(b), using both the Couette and vane measurements, the fluidic yield stress increases generally linearly with an increase in the density. For the first three experimental days, it was not possible to remove the thin water layer from the top of the mud samples, which led to the invariable density values. The yield stress appeared to increase as a result of the settling and consolidation processes. The limitation of the density measurement cannot successfully reflect the increase in the density with the yield stress.

C. The relation between yield stress, density, and S-wave velocity

By plotting the fluidic yield stress and S-wave velocity in Fig. 9(c), we observe that the fluidic yield stress and S-wave velocity are positively correlated. It is noticed that the increase in the S-wave velocity lagged behind the increase in the yield stress during the early stages of the fluid-mud settling. That is, there is no apparent change in the S-wave velocity from day 0 to day 2, whereas the fluidic yield stress increased during those days. A possible explanation is that the S-wave velocity is determined by the density, shear modulus, and yield stress. The observed stability of the S-wave velocity in the early stage of the fluid-mud settling could be connected to the relative stability of density during the same period [Fig. 9(d)]. Comparing the P-wave velocity change and S-wave velocity change, we find that the S-wave velocity change reflects the density change of the mud samples at least after day 3. The constant P-wave velocity during the consolidation process implies that the P-waves are not sensitive enough to the observed small change of the density. This agrees with the study by Hamilton and Bachman (1982), which suggested that a P-wave velocity change can only be detected after a significant change of the density of marine sediments. The increase in density as a result of the reduction in porosity is the main factor causing the increase in the S-wave velocities. Finer-grained sediments experience a significantly higher increase in the velocity than coarser-grained sediments with an effective pressure increase because of a higher porosity reduction in the finer-grained sediments.

https://doi.org/10.1121/10.0005039

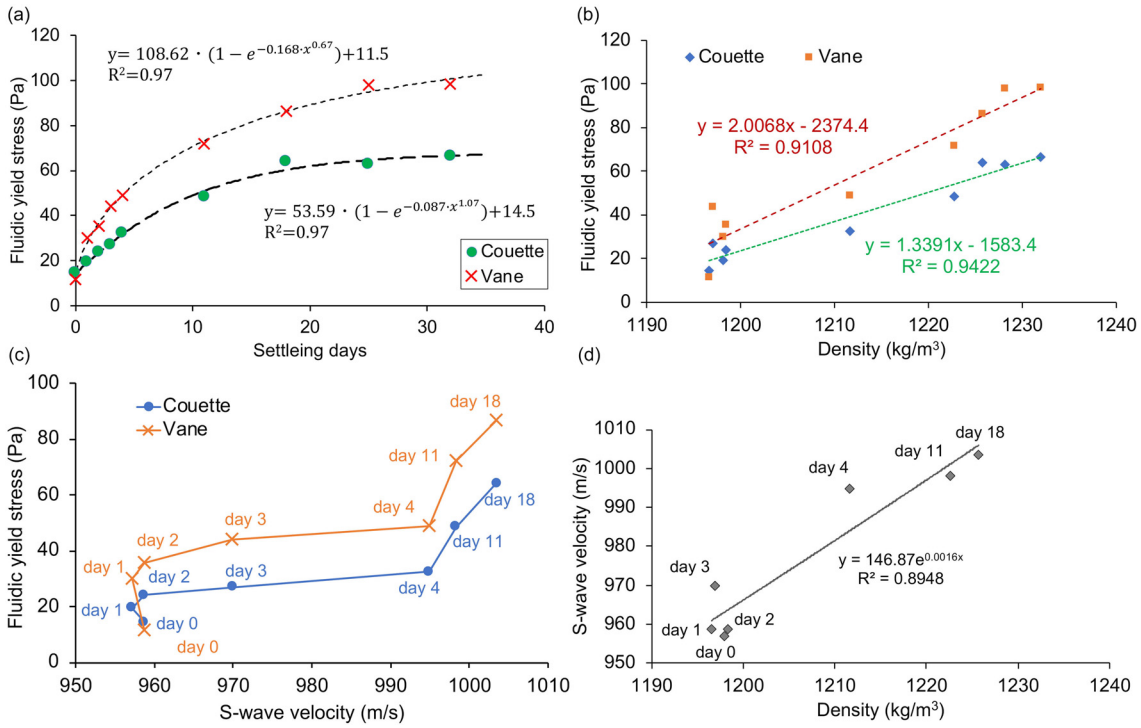

FIG. 9. (Color online) (a) The temporal change of the fluidic yield stress using measurements with the Couette [Fig. 8(a)] and vane geometries [Fig. 8(b)]. The point measurements are fitted using regression analysis. (b) The fluidic yield stress versus density using measurements of the Couette and vane geometries. (c) The fluidic yield stress versus S-wave velocity using measurements the Couette and vane geometries. (d) The S-wave velocity versus density.

D. Analyzing seismic reflections using velocity semblances

The aim of our reflection experiments is to monitor the temporal change of the seismic reflections with mud settling and retrieve ghost reflections from only inside the mud layer. We use the method of SI for removing the water portion of a reflected signal and retrieving reflections only inside the fluid-mud layer.

Following standard resource-exploration processing, we use PPPP, PPSP, and PSSP as the main targets. We perform velocity semblance analysis on the recorded common-source gathers to try to identify the changes in the propagation velocities with mud settling. Semblance analysis, also called velocity-spectrum analysis, has played an important role in velocity analysis of seismic data (Fomel, 2009). Using semblance analysis helps suppress noise and extract the primary reflections. Semblance analysis uses varying values of the effective moveout velocity to stack along reflection hyperbolas placed at different points along the time axis of a recorded seismic data, in our case, the common-source gather (Yilmaz, 2001). The result of the semblance analysis can be plotted as a function of the intercept time and stacking velocity, which shows maxima highlighting reflection events characterized by a specific effective velocity.

The distribution of the maxima in the velocity semblance in Fig. 10 exhibits separated regions for PPPP, PPSP, and PSSP. During the mud settling, the reflection PPPP arrival exhibits the largest semblance compared to the other two primary reflections because the principal portion of the energy is partitioned to PPPP. Its two-way traveltime ranges between 0.22 and 0.24 ms, meaning that the apparent velocity of PPPP appears to be between 1400 and 1600 m/s for all of the settling periods. Because the S-wave velocity is lower than the P-wave velocity in mud, PPSP arrives at receivers later than PPPP. Similarly, PSSP arrives later at the receiver than PPSP because PSSP contains two S-wave propagation parts. The apparent velocity of PPSP ranges between 1250 and 1350 m/s, whereas the apparent velocity of PSSP is the lowest, as expected, and ranges between 1000 and 1100 m/s. As can be seen from the plots in Fig. 10, other than the mentioned velocity ranges, it is difficult to extract more exact quantitative information about the velocities.

Although we do not show this here, the semblance analysis can be applied to the reflection from the water/fluid–mud interface [magenta arrival in Fig. 3(a)] to estimate the velocity of the water. After that, this value can be used to map exactly the depth to the interface.

By examining the semblances, we also compare the energy of PPPP, PPSP, and PSSP and its temporal evolution during the settling period of 12 days. Starting from day 0 immediately after placing the mud in the tank and going to day 11, the energy of PPPP appears to be the largest portion present. In comparison, it is noticed that the semblances of PPSP and PSSP, which include the P-to-S converted portion, pronouncedly change with the settling time, implying that the energy conversion from the P-wave to S-wave is strengthened with mud consolidation. During the first

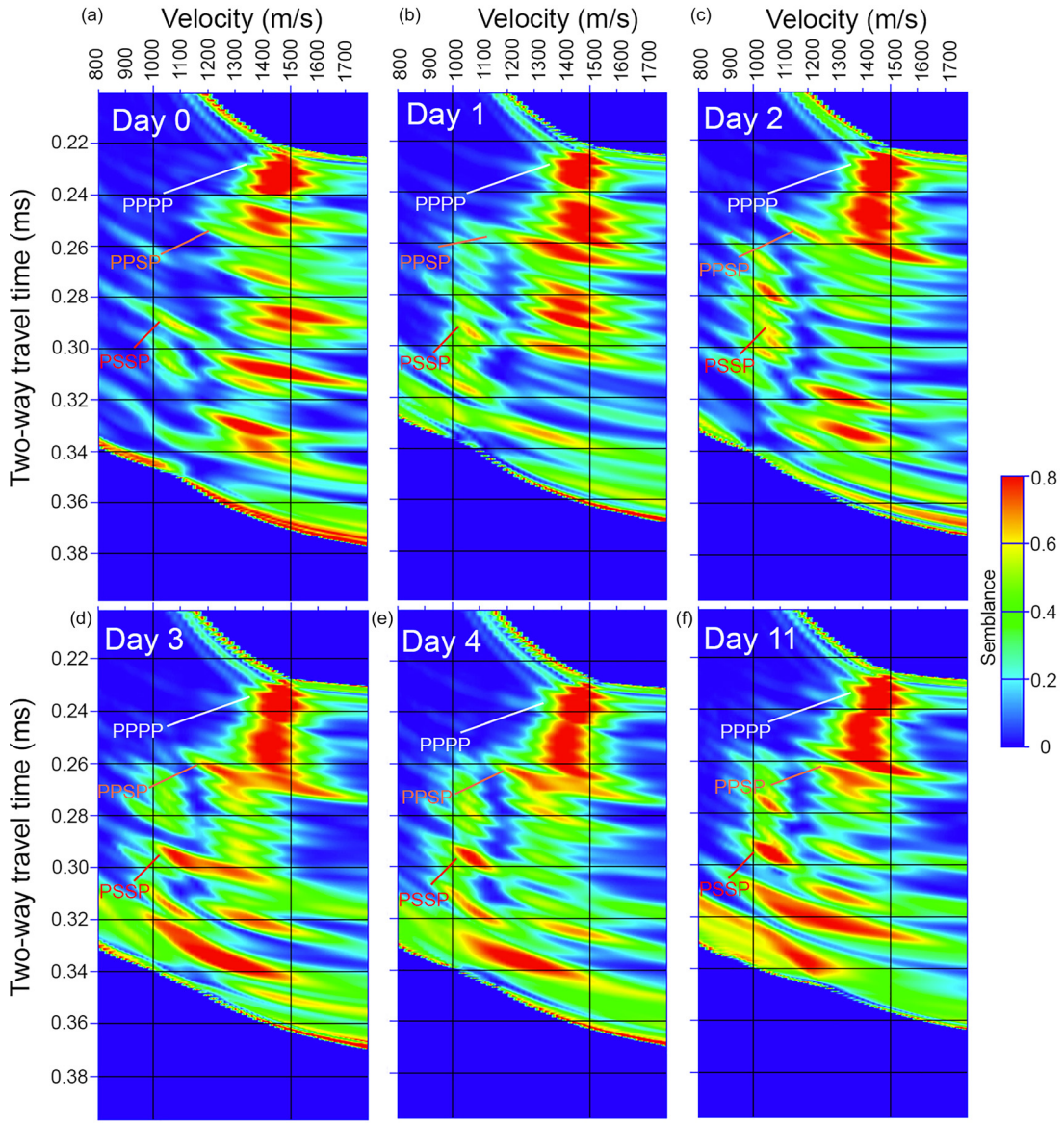

FIG. 10. (Color online) The temporal changes of the seismic reflections PPPP, PPSP, and PSSP from the fluid mud and water layer obtained from the semblance analysis of the common-source reflection gathers measured at (a) day 0, (b) day 1, (c) day 2, (d) day 3, (e) day 4, and (f) day 11.

3 days, PPSP and PSSP exhibit low semblance amplitudes [Figs. 10(a)–10(c)], suggesting that only small portions of the propagating energy convert from P- to S-waves. With the progress of the settling, larger portions of the propagating energy convert from P- to S-waves due to the increasing difference of the density of water and mud and the intensifying compaction of mud.

The semblance analysis illustrates that the temporal evolutions of the P- and S-waves and, thus, the consolidation of the fluid mud can be identified and qualitatively monitored. However, the semblance analyses of PPPP, PPSP, and PSSP can only illustrate certain ranges for the velocity rather than allow precise velocity picks with the settling time because of the limitation of the method. To increase the resolution of the semblance, dense sampling along the complete range of offsets (from near to far) would be needed with minimum interference from other events, e.g., water multiples, refractions. Furthermore, the estimated velocities are apparent velocities influenced also by the presence of the water layer. To obtain good estimates of the fluid-mud velocities, semblance analysis of the water layer would be required. To obviate the need for the latter and, therefore, the influences of variables, such as salinity and temperature, of the water layer, we proceed to retrieve ghost reflections from inside the mud layer.

E. Retrieval of ghost reflections inside the mud layer

We use two identical sources to retrieve ghost reflections as described in Sec. II. First, we obtain the common-source gathers of source 1 [Fig. 11(a)] and source 2 [Fig. 11(b)]. Next, we apply SI by using the reflections from the mud top from source 2 [Fig. 11(c)] to eliminate P-wave propagation paths inside the water layer of the three primary

https://doi.org/10.1121/10.0005039

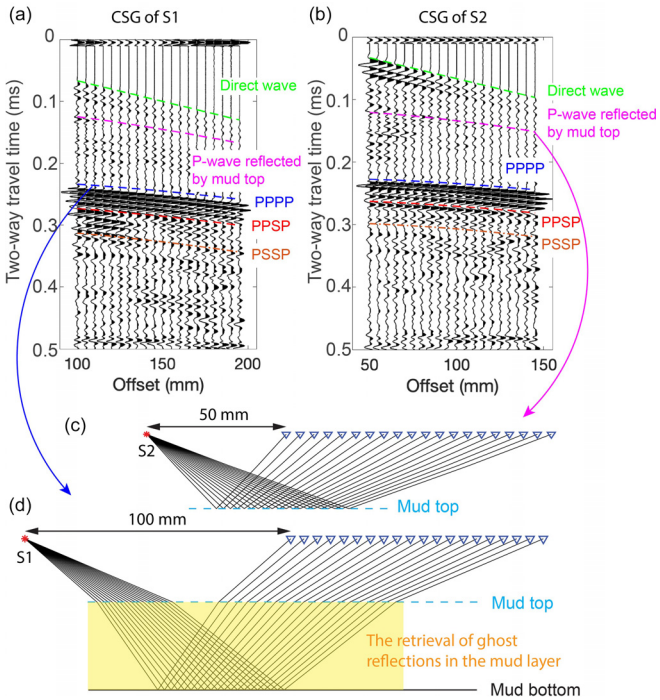

FIG. 11. (Color online) The reflection common-source gathers (CSGs) from (a) source 1 and (b) source 2 used for retrieval of a ghost reflection inside the mud layer. Sketch of (c) the travelpaths of the P-waves reflected by the mud top in CSG from S2 and (d) the travelpaths of PPPP in CSG from S1. The highlighted part in (d) shows the parts of the wavefield contributing to the retrieval of the ghost reflection. The PPSP and PSSP arrival waves have similar structures to those of PPPP and, thus, the retrieval process is essentially the same.

reflections PPPP, PPSP, and PSSP from source 1 [Fig. 11(d)]. In this way, the ghost reflections PP, PS, and SS, represented by the segments 2 and 3 in Fig. 4, inside the mud layer are retrieved.

1. F-K filter

In addition to the seismic reflections of interest, direct waves are also recorded when performing the measurements. The direct waves, labeled by a green line in Fig. 11(b), partly overlap with the seismic waves being reflected by the mud top. This could negatively influence the retrieval of the ghost reflections, e.g., resulting in an erroneous retrieved arrival time. To avoid that, we want to suppress the direct waves. For that purpose, we use a slope filter in the frequency-wavenumber (F-K) domain to filter out the direct waves before applying SI. In Figs. 12(a) and 12(c), the spot with the highest amplitude indicates the primary reflection PPPP as this portion contains the major part of emitted energy, and the center frequency of the source is nearly 100 kHz. The energy pertaining to the direct waves is to the right of the dashed line in Fig. 12(a). As can be seen in Fig. 12(c), the application of the slope filter removes the direct-wave energy while the reflections of interest are preserved. The effect of the F-K filtering can be appreciated by comparing the original and filtered common-source gathers in the time-space domains in Figs. 12(b) and 12(d), respectively, which shows

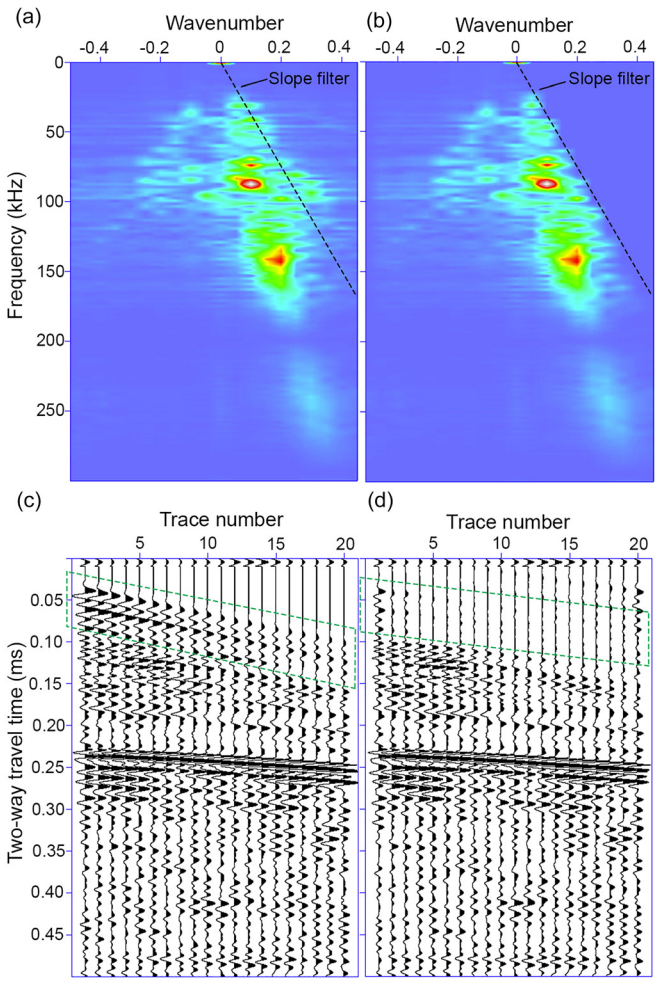

FIG. 12. (Color online) (a) The Fourier spectrum of the common-source gather of source 2 before applying a slope filter in the F-K domain. (b) Wiggle plot of the common-source gather of source 2 before applying a slope filter; waves in the green polygon represent the direct waves that need to be eliminated before applying SI for constructing ghost reflections. (c) Fourier spectrum of the common-source gather of source 2 after applying a slope filter in the F-K domain. (d) Wiggle plot of the common-source gather of source 2 after applying a slope filter; direct waves and noises in the green polygon have been removed.

that the furthest offsets of the P-wave reflection from the mud top are now revealed. This will ensure a more accurate retrieval of the ghost reflections.

2. Applying SI for ghost-reflection retrieval

We apply SI for the retrieval of ghost reflections to the measurements from day 11. To retrieve clear ghost reflections, it is advisable to apply SI separately to each of PPPP, PPSP, and PSSP (Draganov *et al.*, 2012; Draganov *et al.*, 2013). We do this by identifying the three primary reflections PPPP, PPSP, and PSSP from S1 [Fig. 13(a)] and extracting each one of them separately by applying tapered top and bottom muting. We then also extract in a similar way, the P-wave reflection from the mud top from S2. To retrieve the ghost reflections as highlighted in Fig. 11(d), we continue to apply SI by cross-correlating the primary reflections PPPP, PPSP, and PSSP [Fig. 13(a)] with the reflection

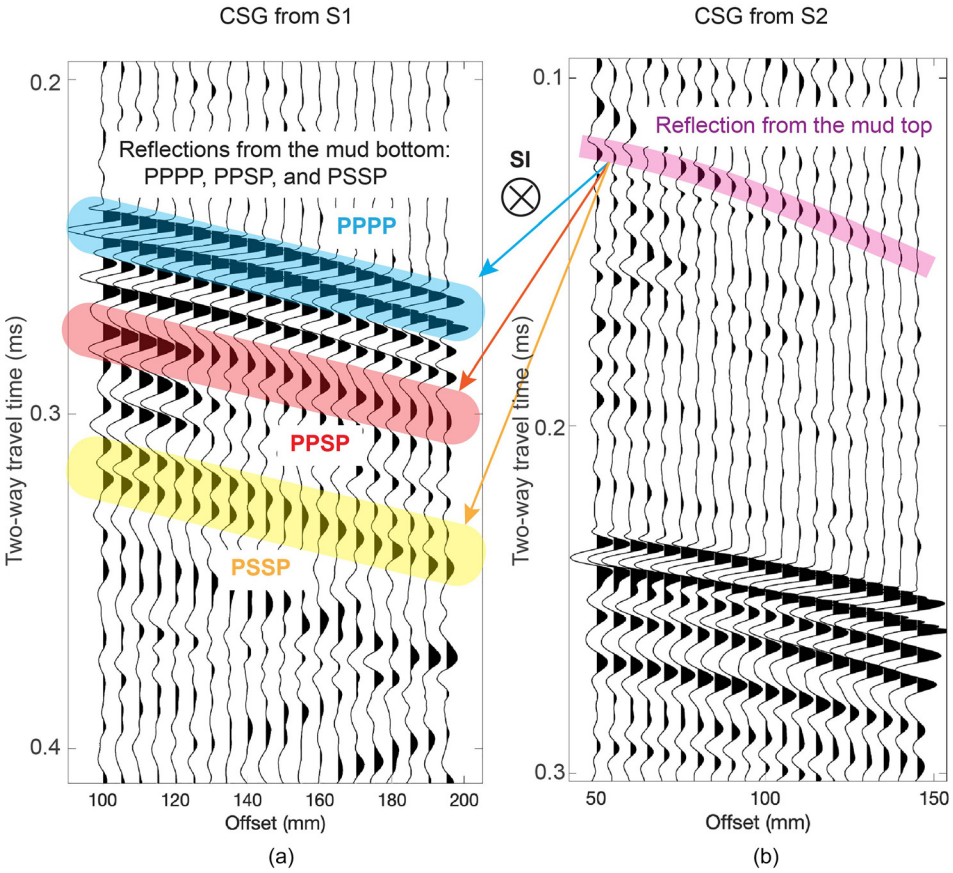

FIG. 13. (Color online) The highlighted reflections in the common-source gather from (a) source 1 and (b) source 2 and are extracted by muting and used for retrieval of the ghost reflection. The explanations of applying SI are shown in Fig. 4.

from the mud top [Fig. 13(b)]. The correlation results, the so-called correlation gathers, are shown in Figs. 14(a), 14(c), and 14(e).

The final step of the SI retrieval process is the summation over the receiver positions (Wapenaar and Fokkema, 2006). The summation results in constructive interference inside the stationary-phase region (Snieder, 2004), which retrieves the desired arrivals. For the correlated traces inside the stationary-phase region [yellow rectangles in Figs. 14(a), 14(c), and 14(e)], we can effectively write that the traveltime of the ghost PP reflection, obtained by cross-correlating PPPP from source 1 with $P_{mud\text{-}top}$ (P-wave from source 2 reflected by the mud top), is $PP = PPPP - P_{mud\text{-}top}$. In a similar manner, the travetime of the ghost reflections PS and SS are $PS = PPSP - P_{mud\text{-}top}$ and $SS = PSSP - P_{mud\text{-}top}$, respectively.

Outside the stationary-phase region, the summation results in destructive interference. If the receiver boundary were closed, the contribution of the signals outside the stationary-phase region would be completely eliminated. Because we have an open boundary, artefacts will be retrieved as a result of the summation. To avoid that, we stack the traces in the correlation panels only inside the stationary-phase region. The final retrieved ghost reflections are shown in Figs. 14(b), 14(d), and 14(f). Using the two-way traveltimes of these ghost reflections and because we know the thickness of the mud layer and distance between the ghost source and ghost receivers, we can estimate the P- and S-wave velocities inside the mud later using the picked two-way traveltimes. We pick the two-way traveltime at the onset of the arrivals as shown in Fig. 14. We estimate the P-wave velocity using the ghost reflection PP as 1592 m/s, the S-wave velocity using the ghost reflection SS as 995 m/s, and while using the ghost reflection PS and the already estimated P-wave velocity, we obtain an estimate of 990 m/s for the S-wave velocity. The uncertainties in the velocity calculation may come from the initial positions of source transducers, which are ±0.5 mm. Uncertainties in the positioning of the receiver transducers are eliminated in the retrieval process of the ghost reflections because of the summation over the receiver positions. The uneven surface of the fluid-mud layer can also be a source of uncertainty. If the fluid-mud surface is uneven, the ghost source and/or receiver might fall into a local trough or peak of the surface and, thus, be at a level different than the one we measured. Because of this, in our laboratory setup, we try to minimize such uncertainties by ensuring that the surface of the mud layer is very flat during the preparation.

F. Comparison of the reflection measurements, transmission measurements, and GS modeling

The seismic transmission measurements and reflection measurements are conducted to investigate the feasibility of characterizing and monitoring the fluid mud during the settling. As expected, the transmission measurements present results with good quality that allow easy characterization and monitoring of the fluid mud. For practical use in ports

https://doi.org/10.1121/10.0005039

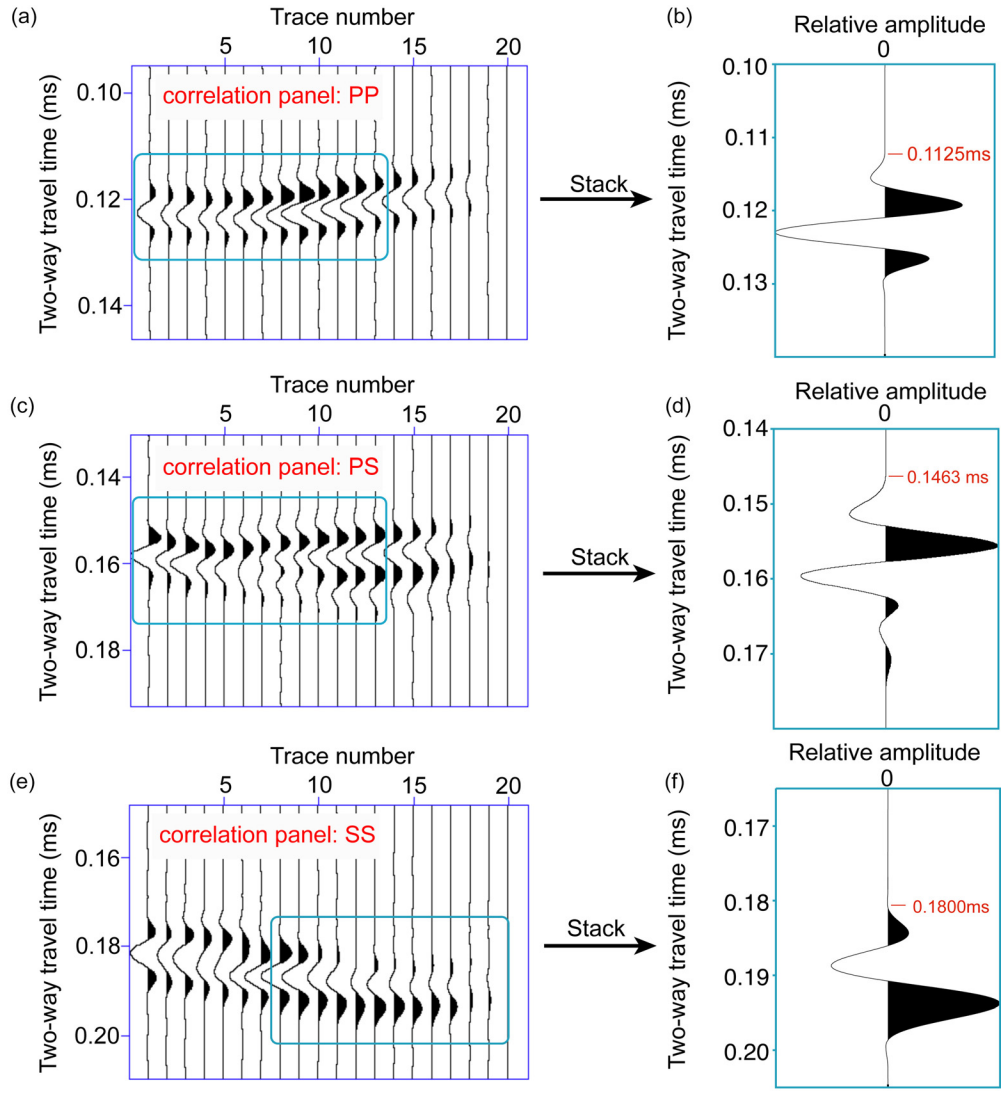

FIG. 14. (Color online) The correlation panels obtained from correlating the traces with the P-wave reflection from the mud top in Fig. 13(b) with the traces with the (a) PPPP, (c) PPSP, and (e) PSSP arrivals from Fig. 13(a). Yellow rectangles indicate the stationary-phase regions. Stacking the traces inside these regions retrieves the (b) PP, (d) PS, and (f) SS ghost reflections inside the mud layer.

and waterways, they would require borehole-like measurements at multiple points, for example, with distributed acoustical sensing (helically wounded) from multiple source points to allow tomographic inversion for improved spatial resolution. This makes their practical application less straightforward.

On the other hand, performing reflection measurements in a marine environment using the seismic-exploration practices would be straightforward. The laboratory measurements we performed show that the reflection measurements with the velocity analysis using semblances could be used for qualitative characterization and monitoring of the settling process. At the same time, the P- and S-wave velocities estimated from the retrieved ghost reflections PP and SS are nearly the same as the transmission measurements. The values from the transmission measurements are 1570 and 998 m/s; from the ghost reflections, the estimated values are 1592 and 995 m/s for the P- and S-wave velocities, respectively. The relative differences are 1.4% and 0.3%, respectively. Why the relative difference for the P-wave is higher needs to be investigated further. The S-wave velocity estimated using the ghost reflection PS is 990 m/s, meaning a relative difference compared to the transmission measurements of 1.0%. This cannot be explained only with the relative difference in the P-wave velocity. The extra difference might be coming from the phase change of the signals inside the stationary-phase region [Fig. 14(c)]. This also needs to be investigated further.

The above comparison shows that reflection measurements with ghost-reflection analysis have a very good potential for quantitative characterization and monitoring of fluid mud. The reliable estimation from all three ghost reflections PP, PS, and SS would allow estimating the velocity and thickness of the mud layer simultaneously.

We compare the P- and S-wave velocities from our measurements with the modeling results using the grain

shearing (GS) theory (Buckingham, 1997). We use the GS expressions of Buckingham (1997),

$$C_p = C_o\sqrt{(1+\chi_p)}, \tag{1a}$$

$$\chi_p = \frac{\gamma_p + \frac{4}{3}\gamma_s}{\rho_o C_o^2}, \tag{1b}$$

$$C_o = \sqrt{\frac{B_w B_s}{[\beta B_s + (1-\beta)B_w][\beta\rho_w + (1-\beta)\rho_s]}}, \tag{1c}$$

$$C_s = \sqrt{\frac{\gamma_s}{\rho_o}}\frac{(\omega T)^{n/2}}{\cos\left(\frac{n\pi}{4}\right)}. \tag{2}$$

The parameter values are listed in Table I and some parameters are from the study of Ballard and Lee (2016) and Buckingham (2005). Using the above equations, for a frequency of 1 MHz, we obtain a P-wave velocity of 1580 m/s and S-wave velocity of 947 m/s. The P-wave velocity is very close to the value in our measurements. The modeled S-wave velocity is slightly slower than the values for the S-wave velocity that we measured. This shows that the GS modeling can provide a very good fit to the seismic propagation velocities in fluid mud. Still, the GS theory does not account for the viscous effect of the saturated, unconsolidated granular medium because the viscous dissipation effect can be negligible at higher frequencies. The viscous grain shearing (VGS) theory (Buckingham, 2007) incorporates the viscous effects to bridge the strain-hardening to viscous saturation and is of interest for modeling fluid mud in future studies.

IV. CONCLUSION

Using laboratory rheological and ultrasonic measurements, we investigated the possibility to characterize the fluid-mud behavior during settling. The fluid mud that we used was taken from the Calandkanaal in the Port of Rotterdam. We observed that the fluidic yield stress gradually increased with the settling time during the 32-day period approaching a certain maximum exponentially from below. During the same period, the density initially appeared to stay stable due to the limitation and difficulty of dewatering during the density measurement. However, after the fourth day, the artifact of the stable density was resolved when the initial water layer disappeared. The density was found to increase and started approaching a certain maximum from below. The density and fluidic yield stress exhibited a possible linear relation, except for the first few days. Using transmission ultrasonic measurements, we estimated the propagation velocity of the longitudinal (P) and transverse (S) waves through the fluid mud during the first 18-day settling period. We observed that the P-wave velocity was practically the same, whereas the S-wave velocity started increasing after the second day. We found that the fluidic yield stress and S-wave velocity are positively correlated with the S-wave velocity lagging behind the increase in the yield stress during the early stages of the fluid-mud settling, possibly related to the relative stability of the density during the same period. The positive correlation of the yield stress and S-wave velocity indicates that the S-wave velocity could be used as a tool to indicate the change of the yield stress. More studies are needed to better quantify the mutual correlations between the S-wave velocity and yield stress.

We also performed ultrasonic reflection measurements to mimic standard marine seismic-exploration practice. Using semblance velocity analysis, we showed that seismic reflection measurements could be used for qualitative characterization of the settling process of the fluid mud during the 12-day observation period. Such measurements, though, are influenced strongly by the conditions (temperature, salinity) of the water layer covering the mud. We showed that the kinematic influence of the water layer can be completely eliminated by application of SI to retrieve the P- and S-wave reflections from inside the fluid-mud layer only. We estimated the P- and S-wave velocities to be nearly the same as those estimated from the transmission measurements with relative differences of 1.4% and 0.3%, respectively.

Our laboratory ultrasonic measurements indicate that seismic transmission and reflection measurements could be very useful for the characterization and monitoring of fluid mud in ports and waterways, with reflection measurements for the retrieval of reflections from inside the fluid mud only possibly being more practical for the characterization of larger areas.

TABLE I. Parameter values used in the GS modeling for fluid mud.

Parameter	Symbol	Value
Compressional coefficient (Pa)	γ_p	3.888×10^8
Shear coefficient (Pa)	γ_s	4.588×10^7
Bulk density of fluid mud (kg/m^3)	ρ_o	1200
Density of water (kg/m^3)	ρ_w	998
Density of sediment (kg/m^3)	ρ_s	2460
Bulk modulus of sediment GPa	B_s	38.7
Bulk modulus of water GPa	B_w	2.22
Time (S)	T	1
Angular frequency	ω	6.28×10^6
Material exponent	n	0.2

ACKNOWLEDGMENTS

This research is supported by the Division for Earth and Life Sciences (ALW) with financial aid from the Netherlands Organization for Scientific Research (NWO) with Grant No. ALWTW.2016.029. The project is carried out within the framework of the MUDNET academic network.[1] We thank the three anonymous reviewers for their constructive comments, which helped improve the manuscript.

APPENDIX

See Fig. 15 for the summary of the particle-size distributions of the fluid-mud samples used.

https://doi.org/10.1121/10.0005039

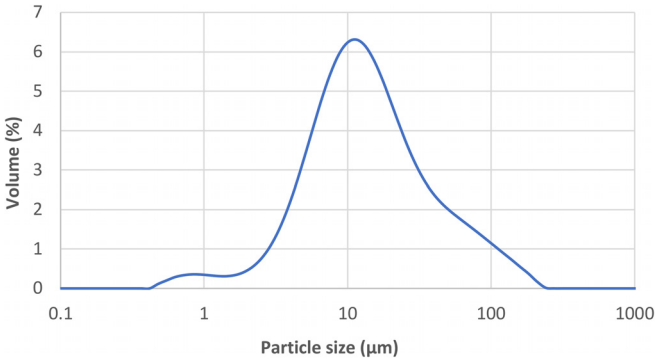

FIG. 15. (Color online) The particle-size distribution of the fluid-mud sample.

[1]See https://www.tudelft.nl/mudnet/ (Last viewed 4/30/2021).

Abril, G., Riou, S. A., Etcheber, H., Frankignoulle, M., De Wit, R., and Middelburg, J. J. (**2000**). "Transient, tidal time-scale, nitrogen transformations in an estuarine turbidity maximum—Fluid mud system (The Gironde, South-west France)," Estuarine, Coastal Shelf Sci. **50**(5), 703–715.

Ballard, M. S., Lee, K. M., and Muir, T. G. (**2014**). "Laboratory P-and S-wave measurements of a reconstituted muddy sediment with comparison to card-house theory," J. Acoust. Soc. Am. **136**(6), 2941–2946.

Ballard, M. S., and Lee, K. M. (**2016**). "Examining the effects of microstructure on geoacoustic parameters in fine-grained sediments," J. Acoust. Soc. Am. **140**(3), 1548–1557.

Bowles, F. A. (**1997**). "Observations on attenuation and shear-wave velocity in fine-grained, marine sediments," J. Acoust. Soc. Am. **101**(6), 3385–3397.

Buckingham, M. J. (**1997**). "Theory of acoustic attenuation, dispersion, and pulse propagation in unconsolidated granular materials including marine sediments," J. Acoust. Soc. Am. **102**(5), 2579–2596.

Buckingham, M. J. (**2005**). "Compressional and shear wave properties of marine sediments: Comparisons between theory and data," J. Acoust. Soc. Am. **117**(1), 137–152.

Buckingham, M. J. (**2007**). "On pore-fluid viscosity and the wave properties of saturated granular materials including marine sediments," J. Acoust. Soc. Am. **122**(3), 1486–1501.

Carneiro, J. C., Gallo, M. N., and Vinzón, S. B. (**2020**). "Detection of fluid mud layers using tuning fork, dual-frequency echo sounder, and chirp sub-bottom measurements," Ocean Dyn. **70**, 573–590.

Chotiros, N. P. (**2021**). "A porous medium model for mud," J. Acoust. Soc. Am. **149**(1), 629–644.

Coussot, P. (**2014**). "Yield stress fluid flows: A review of experimental data," J. Non-Newtonian Fluid Mech. **211**, 31–49.

Draganov, D., Campman, X., Thorbecke, J., Verdel, A., and Wapenaar, K. (**2009**). "Reflection images from ambient seismic noise," Geophysics **74**, A63–A67.

Draganov, D., Ghose, R., Heller, K., and Ruigrok, E. (**2013**). "Monitoring of changes in velocity and *Q* using non-physical arrivals in seismic interferometry," Geophys. J. Int. **192**, 699–709.

Draganov, D., Heller, K., and Ghose, R. (**2012**). "Monitoring CO2 storage using ghost reflections retrieved from seismic interferometry," Int. J. Greenhouse Gas Control **11**, S35–S46.

Drijkoningen, G., el Allouche, N., Thorbecke, J., and Bada, G. (**2012**). "Nongeometrically converted shear waves in marine streamer data," Geophysics **77**(6), P45–P56.

Fomel, S. (**2009**). "Velocity analysis using AB semblance," Geophys. Prospect. **57**(3), 311–321.

Hamilton, E. L. (**1979**). "Sound velocity gradients in marine sediments," J. Acoust. Soc. Am. **65**(4), 909–922.

Hamilton, E. L., and Bachman, R. T. (**1982**). "Sound velocity and related properties of marine sediments," J. Acoust. Soc. Am. **72**(6), 1891–1904.

Jackson, D., and Richardson, M. (**2007**). *High-Frequency Seafloor Acoustics* (Springer Science and Business Media, Secaucus, New Jersey).

Kimura, M. (**2006**). "Shear wave velocity in marine sediment," Jpn. J. Appl. Phys. **45**(5S), 4824.

King, S., and Curtis, A. (**2012**). "Suppressing nonphysical reflections in Green's function estimates using source-receiver interferometry," Geophysics **77**(1), Q15–Q25.

Kirby, R., Hodge, S. H., and Welp, T. L. (**2016**). "Nautical depth for US navigable waterways: A review," J. Waterway, Port, Coastal, Ocean Eng. **142**(2), 04015014.

Kirichek, A., Chassagne, C., Winterwerp, H., and Vellinga, T. (**2018**). "How navigable are fluid mud layers," Terra et Aqua: Int. J. Public Works, Ports Waterw. Dev. **151**, 1–12.

Kirichek, A., Shakeel, A., and Chassagne, C. (**2020**). "Using *in situ* density and strength measurements for sediment maintenance in ports and waterways," J. Soils Sediments **20**, 2546–2547.

Leurer, K. C. (**2004**). "Compressional-and shear-wave velocities and attenuation in deep-sea sediment during laboratory compaction," J. Acoust. Soc. Am. **116**(4), 2023–2030.

McAnally, W. H., Friedrichs, C., Hamilton, D., Hayter, E., Shrestha, P., Rodriguez, H., Sheremet, A., and Teeter, A., ASCE Task Committee on Management of Fluid Mud. (**2007**). "Management of fluid mud in estuaries, bays, and lakes. I: Present state of understanding on character and behavior," J. Hydraul. Eng. **133**(1), 9–22.

Meredith, J. A., Cheng, C. H., and Wilkens, R. H. (**1987**). *Determining Shear Wave Velocities in Soft Marine Sediments* (Earth Resources Laboratory, Massachusetts Institute of Technology, Cambridge, Massachusetts).

Nichols, M. M. (**1984**). "Fluid mud accumulation processes in an estuary," Geo-Mar. Lett. **4**(3), 171–176.

Shakeel, A., Kirichek, A., and Chassagne, C. (**2020a**). "Rheological analysis of mud from Port of Hamburg, Germany," J. Soils Sediments **20**, 2553–2562.

Shakeel, A., Kirichek, A., and Chassagne, C. (**2020b**). "Yield stress measurements of mud sediments using different rheological methods and geometries: An evidence of two-step yielding," Mar. Geol. **427**, 106247.

Shapiro, N. M., and Campillo, M. (**2004**). "Emergence of broadband Rayleigh waves from correlations of the ambient seismic noise," Geophys. Res. Lett. **31**(7), L07614, http://dx.doi.org/10.1029/2004GL019491.

Snieder, R. (**2004**). "Extracting the Green's function from the correlation of coda waves: A derivation based on stationary phase," Phys. Rev. E **69**(4), 046610.

Snieder, R., Wapenaar, K., and Larner, K. (**2006**). "Spurious multiples in seismic interferometry of primaries," Geophysics **71**(4), SI111–SI124.

Stoll, R. D. (**1977**). "Acoustic waves in ocean sediments," Geophysics **42**(4), 715–725.

Wapenaar, K., and Fokkema, J. (**2006**). "Green's function representations for seismic interferometry," Geophysics **71**(4), SI33–SI46.

Yilmaz, Ö. (**2001**). *Seismic Data Analysis: Processing, Inversion, and Interpretation of Seismic Data* (Society of Exploration Geophysicists, New York).